



EXPERIMENTAL EMISSIVITY DETERMINATION FOR THE STAINLESS STEELS ASTM A 743 CA6NM AND AWS 410 NiMo FOR APPLICATION AT HIGH TEMPERATURES

Matheus Tabata Santos

Universidade de Brasília - Campus Universitário Darcy Ribeiro, S/N - Asa Norte - Brasília - DF, 70910-900
mateustabata@gmail.com

Palloma Vieira Muterlle

Universidade de Brasília - Campus Universitário Darcy Ribeiro, S/N - Asa Norte - Brasília - DF, 70910-900
palloma@unb.br

Guilherme Caribé de Carvalho

Universidade de Brasília - Campus Universitário Darcy Ribeiro, S/N - Asa Norte - Brasília - DF, 70910-900
gcarval@unb.br

Taygoara Felamingo de Oliveira

Universidade de Brasília - Campus Universitário Darcy Ribeiro, S/N - Asa Norte - Brasília - DF, 70910-900
taygoara@unb.br

Leonardo Vasconcelos de Abreu Ruszczyk

Universidade de Brasília - Campus Universitário Darcy Ribeiro, S/N - Asa Norte - Brasília - DF, 70910-900
leonardo1703@gmail.com

Abstract. *Emissivity is the ratio between the radiant hemispherical power emitted by a real body, at an absolute temperature, and the radiant hemispherical power emitted by a black body at the same temperature. The energy emitted is proportional to the fourth power of the object's temperature. Emissivity may vary from 0 (reflected by a mirror) to 1.0 (black body theory). Studies are being carried out at the University of Brasilia to investigate the microstructural behavior of materials used in the repairing of hydroelectric turbines, after several thermal cycles of welding. These studies use thermographic techniques for monitoring the temperature and require that the correct emissivity value for specific materials and surface conditions are used in order to guaranty that the temperatures reported by the radiometric sensors are consistent with the actual temperatures. This study aims to validate an experimental methodology for evaluating the emissivity of the steel ASTM A 743 CA6NM and the AWS 410 NiMo as deposited by a GMAW process at temperatures ranging from 100°C to 1000°C. The experiment consists of heating a small sample of the material with an oxyacetylene torch while a thermocouple, welded on surface of the sample, an infrared sensor and a thermographic camera monitor the surface temperature. During the heating and the cooling process, the sample surface is protected from the air by an argon gas flow directed towards the visualized area. Results consistent with the reported in the literature for similar materials were attained and curves of the emissivity "versus" temperature for the tested materials were produced, providing a basis for proper thermographic temperature monitoring.*

Keywords: *Emissivity, ASTM A 743 CA6NM, GMAW, AWS 410NiMo, thermographic monitoring.*

1. INTRODUCTION

The problem with the application of thermography and non-contact temperature measurement is the correct emissivity determination of the material to be adjusted in radiometric devices, so that the temperature measured in the device is as close as possible to the actual temperature of the radiation emitting surface. Besides the factors that influence the correct temperature measurement, the existence of a gaseous medium between the device and the part observed, for example, the emissivity of the material is mainly responsible for proper temperature measurement, particularly for high temperatures (FLIR Systems, 2004).

Radiation is energy emitted by matter in the form of electromagnetic waves (or photons) as a result of changes in the electronic configuration of atoms or molecules. Unlike conduction or convection, the transfer of energy by radiation does not require a material medium to propagate. It is a faster form of energy transfer, occurring at the speed of light in the medium and do not suffer attenuation in vacuum (ÇENGEL, 2003).

Thermal radiation is a form of electromagnetic radiation emitted by bodies due to their temperature. It differs from other forms of radiation such as X-rays, gamma rays, microwaves and radio waves that are not related to temperature. All bodies that are above absolute zero emit thermal radiation (ÇENGEL, 2003). It is considered a volumetric phenomenon, and all solids, liquids and gases emit, absorb or transmit thermal radiation in varying ranges. However, it is usually considered to be a surface phenomenon, as the incident radiation is typically absorbed in the bodies within a

Matheus Tabata Santos, Palloma V. Muterle, Guilherme Caribé de Carvalho, Taygoara F. de Oliveira and Leonardo V. de A. Ruszczuk. Experimental Emissivity Determination for the Stainless Steels CA-6NM and 410 NiMo for Application at High Temperatures

small distance from the surface and the radiation emitted within these solids considered opaque to thermal radiation as metals, woods and stones is strongly absorbed by adjacent molecules (INCROPERA et al., 2007) and fail to reach the surface (ÇENGEL, 2003). The radiation that is emitted by solid or liquid originates from molecules that are at a distance of approximately 1 μm of the exposed surface (INCROPERA et al., 2007).

In 1879, Joseph Stefan determined experimentally the emissive power radiant energy emitted by a black body per unit time and unit surface area, expressed as

$$E_b(T) = \sigma T^4, \quad (1)$$

where $\sigma = 5,67 \times 10^{-8} \text{ W/m}^2 \cdot \text{K}^4$ is the Stefan-Boltzmann constant and T is the absolute temperature of the surface, in K. Equation (1) is called the Stefan-Boltzmann law and provides full emissive power of a blackbody at a given temperature, which is the sum of all the radiation emitted at all wavelengths, λ (ÇENGEL, 2003).

Later in 1901, Max Planck developed in conjunction with his famous quantum theory, a relation for the spectral emissive power of a black body, known as the law (or distribution) of Planck, expressed as

$$E_{\lambda,b}(\lambda, T) = \frac{C_1}{\lambda^5 [\exp(C_2/\lambda T) - 1]} \quad (2)$$

where: $\lambda = \text{wavelength}$, $C_1 = 2\pi h c_0^2 = 3,742 \times 10^8 \text{ W} \cdot \mu\text{m}^4/\text{m}^2$, $C_2 = h c_0/k = 1,439 \times 10^4 \mu\text{m} \cdot \text{K}$

For engineering calculations, it is generally desirable to have surface properties which represent the effective thermal radiation emitting capability of the material. Thus, the so called spectral hemispherical emissivity is defined by the Equation (3), as follows

$$\varepsilon_\lambda(\lambda, T) = \frac{E_\lambda(\lambda, T)}{E_{\lambda,b}(\lambda, T)}. \quad (3)$$

The total hemispherical emissivity, which represents the average emissivity over all possible wavelengths and directions, is defined as

$$\varepsilon(T) = \frac{E(T)}{E_b(T)}. \quad (4)$$

The total power hemispherical emissivity for a surface is defined as the rate at which radiation is emitted per unit area in all possible wavelengths and all possible directions. Mathematically,

$$E(T) = \int_0^\infty E_\lambda(\lambda, T) d\lambda. \quad (5)$$

Substituting the Eq. (5) and Eq. (3) into Eq. (4), it is possible to demonstrate that:

$$\varepsilon(T) = \frac{\int_0^\infty \varepsilon_\lambda(\lambda, T) E_{\lambda,b}(\lambda, T) d\lambda}{E_b(T)}. \quad (6)$$

If a surface's spectral emissivities are known, it then becomes simple to calculate emissive characteristics. If $\varepsilon_\lambda(\lambda, T)$ is known, for example, one can use the equations 2 and 3 to determine the power spectral emissivity of the surface at any wavelength and temperature. Similarly, if $\varepsilon(T)$ is known, one can use equations 1 and 4 to determine the total power emitted by the surface at any temperature (INCROPERA et al., 2007).

The real surfaces do not have a perfectly diffuse emission, as can illustrated in Figure 1, which show the dependence of the total directional emissivity ε_θ with the direction θ for non-conductive and conductive materials.

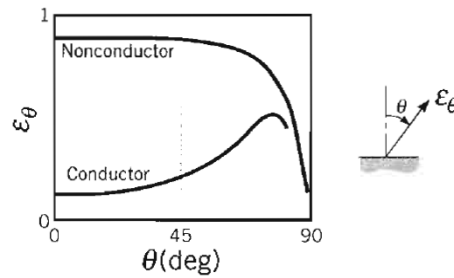


Figure 1: Representative directional distributions of the total directional emissivity (INCROPERA et al., 2007).

An important implication of Fig. 1 is that although there are preferred directions for emitting thermal radiation, the full hemispherical emissivity $\varepsilon(T)$ is not substantially different from normal emissivity $\varepsilon_n(T)$, corresponding to $\theta = 0$, and thus, the approximation shown in Eq. (7) is valid:

$$\varepsilon(T) \approx \varepsilon_n(T). \quad (7)$$

As well as the emissivity varies with wavelength, representative spectral distributions are illustrated in Fig. 2. The way that $\varepsilon_\lambda(T)$ varies with λ depends on whether the material is a conductor or non-conductor and on its surface characteristics (INCROPERA et al., 2007).

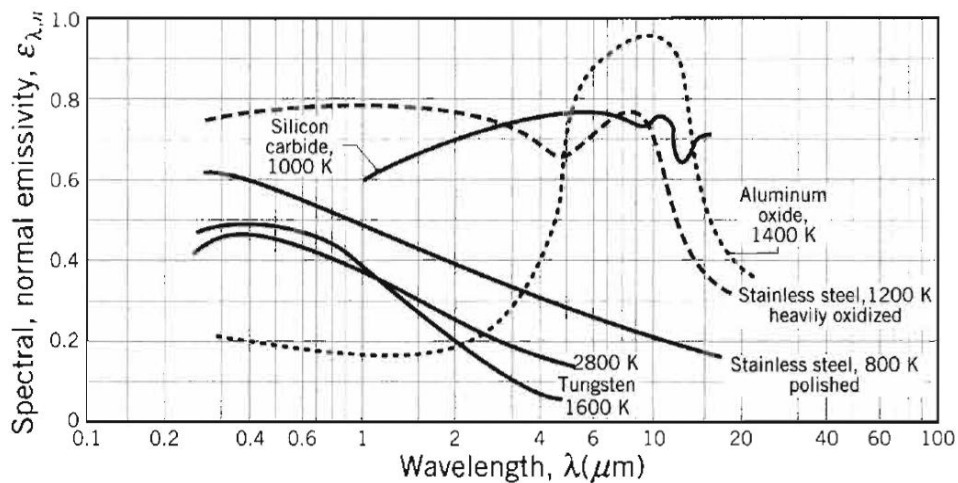


Figure 2: Spectral dependence of the spectral, normal emissivity $\varepsilon_{\lambda,n}$ of selected materials (INCROPERA et al., 2007).

Finally, the emissivity is also a function of temperature, as illustrated in Fig. 3 for some materials selected.

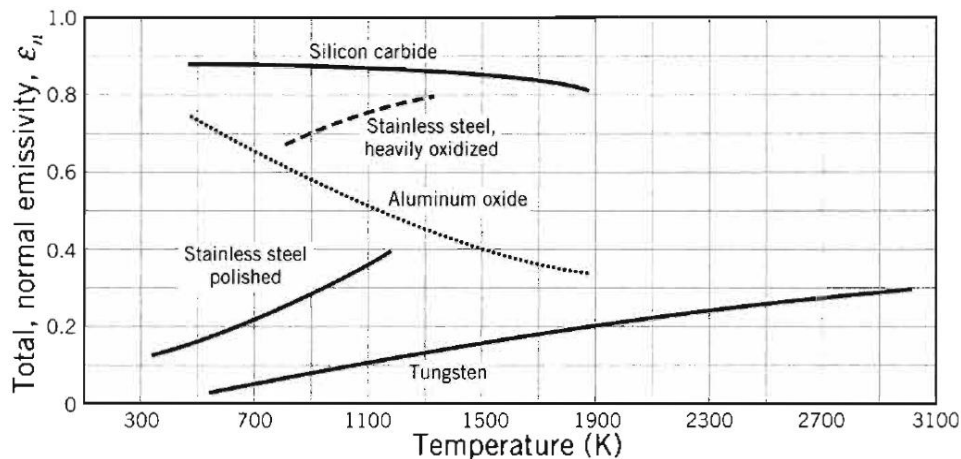


Figure 3: Temperature dependence of the total $\varepsilon_n(T)$, normal emissivity of selected materials (INCROPERA et al., 2007).

Matheus Tabata Santos, Palloma V. Muterlle, Guilherme Caribé de Carvalho, Taygoara F. de Oliveira and Leonardo V. de A. Ruzsczyk. Experimental Emissivity Determination for the Stainless Steels CA-6NM and 410 NiMo for Application at High Temperatures

The spectral irradiance can be defined as the rate at which the radiation of wavelength λ is incident on a surface per unit surface area per unit wavelength interval of $d\lambda$ about λ . It can be incident on all possible directions and may result from several different sources. In the most general case, this irradiation interacts with a semitransparent layer such as water or glass plate.

It can be observed that for a spectral component of irradiation (G_λ), portions of this radiation can be reflected ($G_{\lambda,ref}$), absorbed ($G_{\lambda,abs}$) and transmitted ($G_{\lambda,tr}$). Thus, the radiation balance in the medium can be written as shown in Eq. (8).

$$G_\lambda = G_{\lambda,ref} + G_{\lambda,abs} + G_{\lambda,tr} \quad (8)$$

In most engineering applications, the medium is opaque to incident radiation ($G_{\lambda,tr} = 0$) and the remaining processes of absorption and reflection can be treated as a surface phenomenon (INCROPERA et al., 2007).

The absorptivity is a property which determines the fraction of radiation absorbed by a surface. As the emissivity, the absorptivity is a property difficult to determine, mainly related to its spectral and directional dependence. The hemispherical spectral absorptivity is defined as:

$$\psi_\lambda(\lambda) = \frac{G_{\lambda,abs}(\lambda)}{G_\lambda(\lambda)}. \quad (9)$$

The total hemispherical absorptivity, which represents the average integrated in the directions and wavelengths, is defined as the fraction of the total irradiation absorbed by a surface, mathematically:

$$\psi = \frac{G_{abs}}{G}. \quad (10)$$

The hemispherical spectral reflectance is defined as the spectral fraction of the irradiation which is reflected by a surface:

$$\rho_\lambda(\lambda) = \frac{G_{\lambda,ref}(\lambda)}{G_\lambda(\lambda)}. \quad (11)$$

The total hemispherical reflectivity, which represents the average integrated in the directions and wavelengths, is then defined as:

$$\rho = \frac{G_{ref}}{G}. \quad (12)$$

Similarly, the spectral hemispherical transmittance is defined as the fraction of the spectral irradiation which is transmitted by a surface:

$$\tau_\lambda(\lambda) = \frac{G_{\lambda,tr}(\lambda)}{G_\lambda(\lambda)}, \quad (13)$$

and the total hemispherical transmissivity represents the average integrated property in all directions and wavelengths:

$$\tau = \frac{G_{tr}}{G}. \quad (14)$$

It can be concluded then, from the definitions above and the energy balance on Eq. (8), that for a semitransparent medium:

$$\rho_\lambda + \psi_\lambda + \tau_\lambda = 1 \quad (15)$$

and for properties that are taken as averages across the spectrum, it follows that:

$$\rho + \psi + \tau = 1. \quad (16)$$

The surface radiosity consists on a portion of radiant energy emitted, as a function of the surface temperature itself and a portion of radiant energy reflected by the surface, from the neighborhood (NICOLAU et al., 2008), according to Equation (17) (INCROPERA et al., 2007):

$$J_s = \varepsilon E_{bs} + \rho G_s, \quad (17)$$

where J_s e G_s are the radiosity and the surface irradiance, respectively, and $E_{bs} = \sigma T_s^4$ is the black-body emittance on T_s temperature. The emissivity and the surface reflectivity are, respectively, ε and ρ .

Kirchhoff's law allows to establish an equality between the absorptivity and the emissivity for long wave bands ($\varepsilon = \psi$) (NICOLAU et al., 2008) and, consequently, for opaque surfaces ($\tau = 0$). Then, the Eq. (16) reduces to:

$$\rho = 1 - \varepsilon. \quad (18)$$

Considering the neighborhood as an isothermal cavity, on the T_c temperature, involving the sample surface, then the irradiance G_s is equal to cavity emittance σT_c^4 . It's possible to represent the surface radiosity as follows:

$$J_s = \varepsilon \sigma T_s^4 + (1 - \varepsilon) \sigma T_c^4. \quad (19)$$

The total energy flux incident on the radiometer comes from the emission of the surface with T_s temperature and from the reflection of energy from the neighborhood considered as a cavity with T_c temperature. This sum covers the radiometer and there is no way to separate these plots, being taken simply as emission from the surface. Thus, the emissivity to be adjusted on the equipment so that the temperature reading is the same as the temperature reported by the thermocouple is actually an apparent emissivity. Therefore, it replaces the radiosity of Eq. (19) for surface emittance, using this apparent emissivity (NICOLAU et al., 2008):

$$\varepsilon_{ap} \sigma T_s^4 = \varepsilon \sigma T_s^4 + (1 - \varepsilon) \sigma T_c^4, \quad (20)$$

$$\varepsilon_{ap} = \varepsilon + (1 - \varepsilon) \left(\frac{T_c}{T_s} \right)^4. \quad (21)$$

Equation (21) allows to make important observations. It may be noted that the apparent emissivity (ε_{ap}) approximates the actual emissivity (ε) if the cavity temperature is much lower than the surface temperature and the surface has a high emissivity. As emphasized in the methods of measuring temperature without contact, low emissivity surfaces are difficult to measure (NICOLAU et al., 2008).

The apparent emissivity to be adjusted in radiometers is adjusted for all assays to be equal to unity ($\varepsilon_{ap} = 1$). Therefore, the temperature measured by the radiometer no longer represents the actual temperature of the surface T_s , which is measured by the thermocouple, but necessarily a lower temperature denominated T_r . Thus, Eq. (20) reduces to:

$$\sigma T_r^4 = \varepsilon \sigma T_s^4 + (1 - \varepsilon) \sigma T_c^4 \quad (22)$$

and emissivity is then calculated by the Eq. (23), where temperatures should be computed in Kelvin.

$$\varepsilon = \frac{T_r^4 - T_c^4}{T_s^4 - T_c^4} \quad (23)$$

2. OBJECTIVE

The objective of this work was, through an experimental methodology, to determine the emissivity for surfaces with different materials and different finishing conditions, in particular for ASTM A 743 CA6NM steel and for the AWS 410 NiMo steel as welded, and to investigate the behavior of this radiant property in high temperatures around 1000°C in steps of heating and cooling, under protective gas.

3. METHODOLOGY

As a means to analyze and evaluate the behavior of the material's emissivity at high temperatures, an experimental apparatus was designed to allow the heating of a sample of the material and the simultaneous measurement of temperature, using a K-type thermocouple (welded in the sample's central region), an infrared sensor (model TL-T14-09 with spectral band from 8 to 14 μm and the emissivity parameterized on the maximum value) and an infrared camera

Matheus Tabata Santos, Palloma V. Muterlle, Guilherme Caribé de Carvalho, Taygoara F. de Oliveira and Leonardo V. de A. Ruzczyk. Experimental Emissivity Determination for the Stainless Steels CA-6NM and 410 NiMo for Application at High Temperatures

(emissivity parameterized on the maximum value) along with the use of a device designed with a toroidal format to promote the protection of the surface from a highly oxidizing atmosphere through the continuous flow of argon gas.

The experimental apparatus consists of a wooden base, long enough to meet the distances required by the optics of the radiometer and the length of the thermocouple, with aluminum brackets that allow certain rigidity while adjustments in the three translational axes and one spindle adjusting the rotation angle θ in the case of infrared sensors. Fixation was achieved by means of bolts and butterfly type nuts. The experimental apparatus is illustrated in Fig. 4 and Fig. 5.

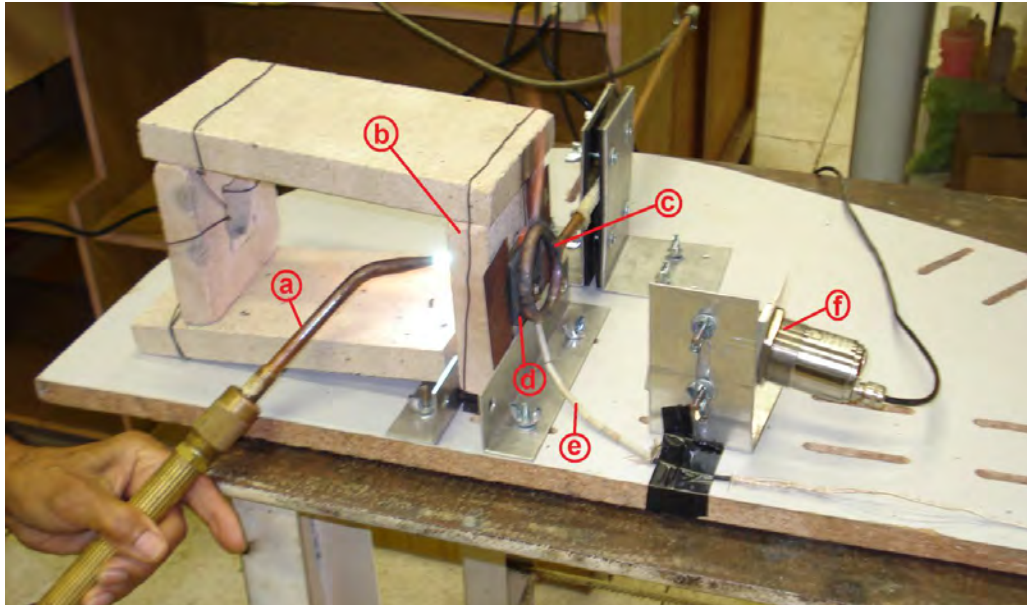


Figure 4: Experimental apparatus. (a) Oxyacetylene flame, (b) Refractory block, (c) Protection gas, (d) Sample to be tested, (e) K-type thermocouple, (f) Infrared sensor.

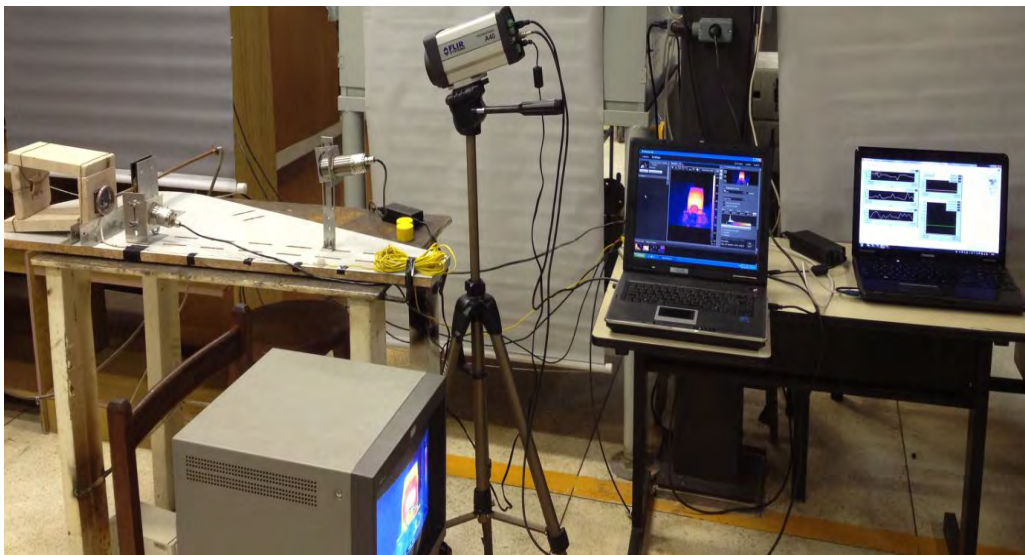


Figure 5: Experimental apparatus used in conjunction with the signal acquisition systems.

Four samples were chosen from materials that are used in the manufacture and repair of turbine blades of hydroelectric power plants, which are: Oxidized Mild Steel, Stainless Steel ASTM A 743 CA6NM, Mild steel with a layer of AWS 410 NiMo added to its surface by GMAW welding and with brushed finish, and lastly, mild steel with a layer of AWS 410 NiMo added to its surface through with GMAW welding with slag and some oxidation (as welded). The mild steel sample was sanded and left exposed to weathering conditions for a natural oxidation. These samples are shown on Fig. 6.

The test samples were cut in rectangular shape measures of 45 x 50 mm and a thickness of 10mm, with uncertainty in the measurements of ± 2 mm.

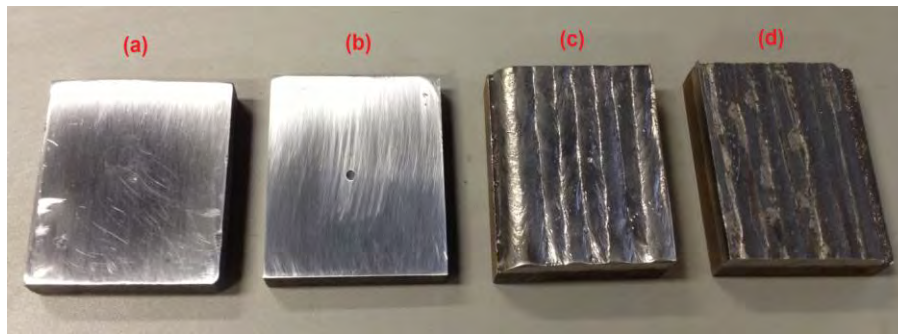


Figure 6: Tested samples. (a) Mild Steel, (b) ASTM A 743 CA6NM, (c) Brushed AWS 410 NiMo, (d) AWS 410 NiMo as welded.

The sample is surrounded by a frame of refractory material to concentrate the heat flow and reduce losses by conduction. To prevent that the radiation provided by the refractory material from reaching the sample and be reflected to the infrared sensor, the sample surface is positioned close to the surface of the refractory or slightly highlighted from this.

First, the sample to be tested is positioned in the frame of refractory material as described in the previous paragraph. Shims are used so that the sample is firmly held in the piece, without damaging the reading of the sensors.

Then, it starts the step of adjusting the sensors. The thermographic filming equipments are installed. The thermocouple is adjusted in a way that its wire does not stay in the camera's field of view. The adjustment of the IR sensor is carried out with the aid of the laser beam emitted by the infrared sensor. The laser spot should be as close as possible to the thermocouple measurement area, but ensuring that the field of view of the radiometric sensors where including only the sample surface.

After the sensors adjustment, the argon cylinder valve is opened for providing the shielding gas protection and the desired flow is adjusted. A flow rate around 16 L/min was found to be sufficient for the desired protection purposes

The oxyacetylene torch is then turned on and a neutral and mild flame is set to prevent the flame from leaking in excess to the sample surface, interfering with the reading of the results and oxidation of the part.

The LabVIEW's "run" button is then pressed together with the thermographic camera recording, giving the start of the acquisition data. The experiment begins with the approach of the torch on the back of the sample along the refractory bricks aimed to limit the heat produced by the flame in other parts of the bench, as illustrated in Fig.4.

The heating ends when it reaches a temperature of about 1000°C (when possible), in which case the temperature increase becomes very slow and there is substantial melting of the material at the back of the sample.

The torch is then turned off and the process of cooling the sample starts with the shielding gas kept on continuously.

4. RESULTS AND DISCUSSION OF RESULTS

The heating and cooling curves for the mild steel sample, provided by a hot rolled flat bar, is illustrated in Fig. 7.

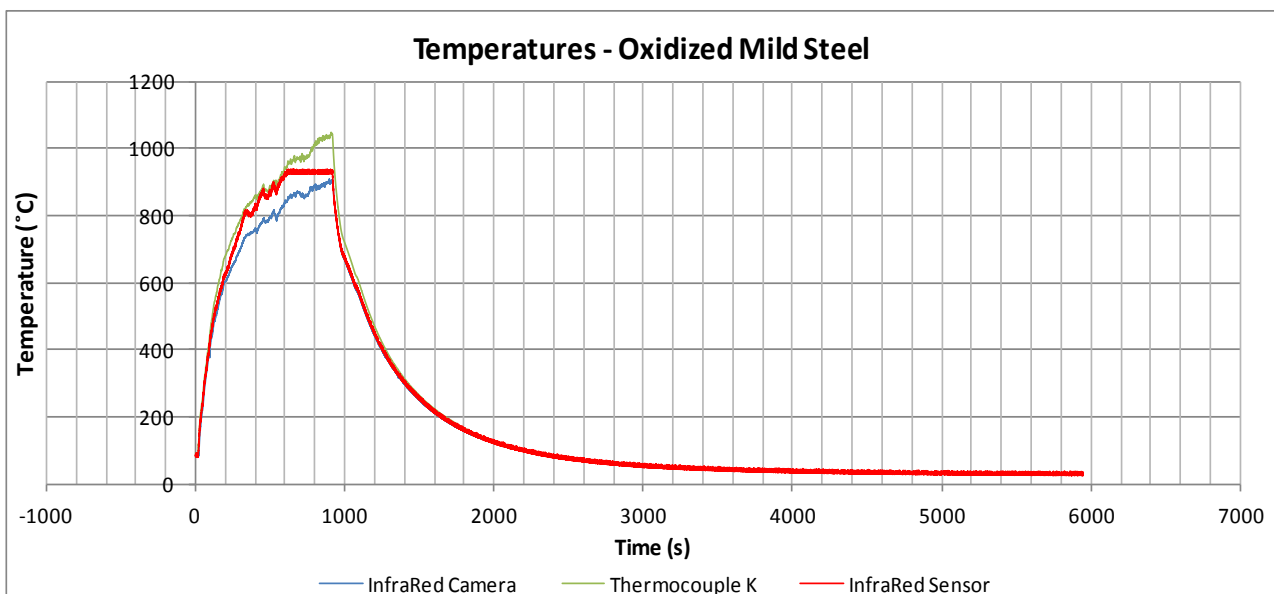


Figure 7: Heating and cooling curves for mild steel.

Matheus Tabata Santos, Palloma V. Muterlle, Guilherme Caribé de Carvalho, Taygoara F. de Oliveira and Leonardo V. de A. Rusczyk. Experimental Emissivity Determination for the Stainless Steels CA-6NM and 410 NiMo for Application at High Temperatures

Only by inspection of the graphs in Fig. 7, mainly in the cooling curves it can be seen that the emissivity for this surface's condition is close to the unity due to the proximity of the three curves and is consistent with the literature for mild steel oxidized (BRAMSON, 1968).

In the cooling curve, observed in Fig. 7, a decrease of cooling rate is noted on all sensors around 700°C, which is believed to be related to material's phase change.

During heating, after 600°C, radiometric sensors and the thermocouple showed considerable difference in measurement. This is due the fact that the oxyacetylene flame passed through the barriers of the ceramic block, interfering in the measurements.

The average emissivity curve for mild steel can be evaluated in the cooling curve and its behavior is shown in Fig. 8. This curve was created based on the ambient temperature, thermocouple temperature data and infrared sensor temperature data.

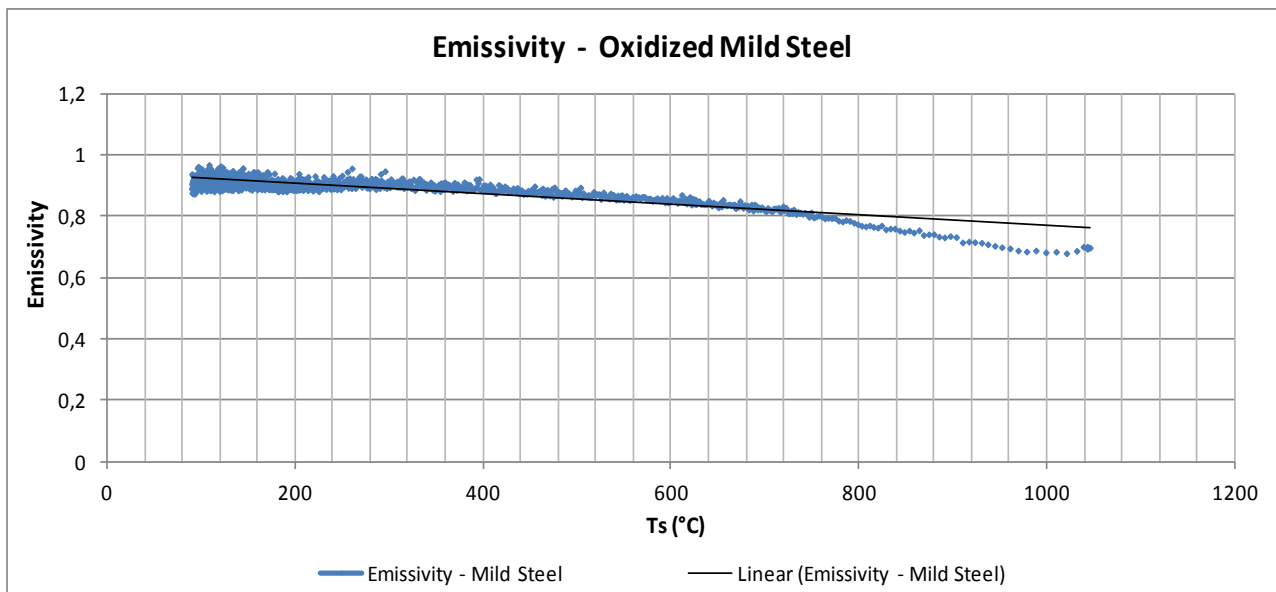


Figure 8: Emissivity curve for mild steel.

In the mild steel emissivity curve is possible to observe a considerable decrease in emissivity at around 700°C, which might be related to a phase change material.

The heating and cooling curves for the ASTM A 743 CA6NM sample is illustrated in Fig. 9.

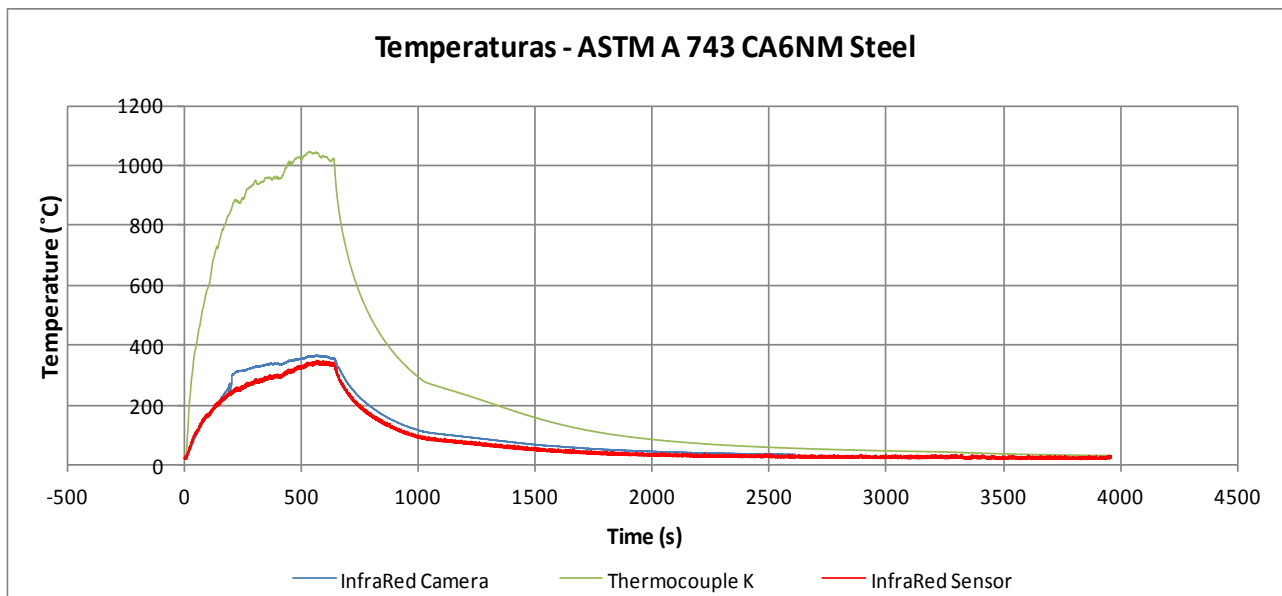


Figure 9: Heating and cooling curves for ASTM A 743 CA6NM Steel.

For the ASTM A 743 CA6NM steel sample, we can observe that the temperature difference informed by thermocouple K compared to the radiometric temperature sensor is very expressive. This fact is expected, since the sample is a martensitic stainless steel and its initial surface is polished.

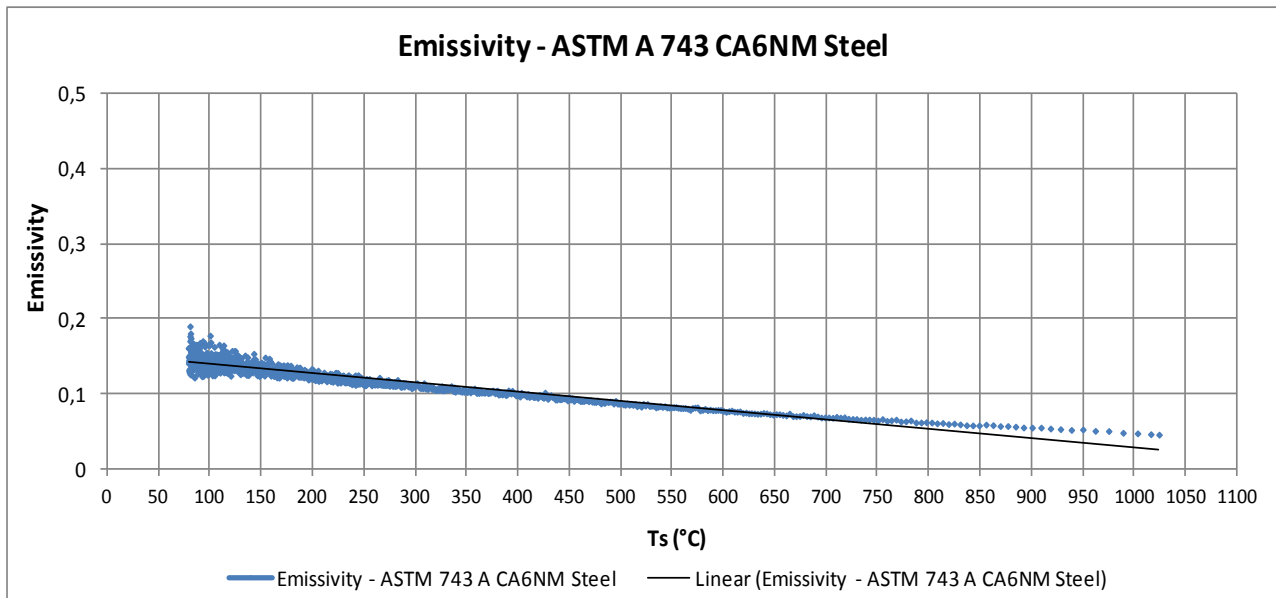


Figure 10: Emissivity curve for ASTM A 743 CA6NM steel.

Due to this fact, the emissivity for this steel is very low, as the literature indicates for stainless steel polished (INCROPERA et al., 2007). Figure 10 reveals the emissivity value and his growth by lowering the temperature. The heating and cooling curves for the brushed AWS 410 NiMo sample is disclosed in Figure 11.

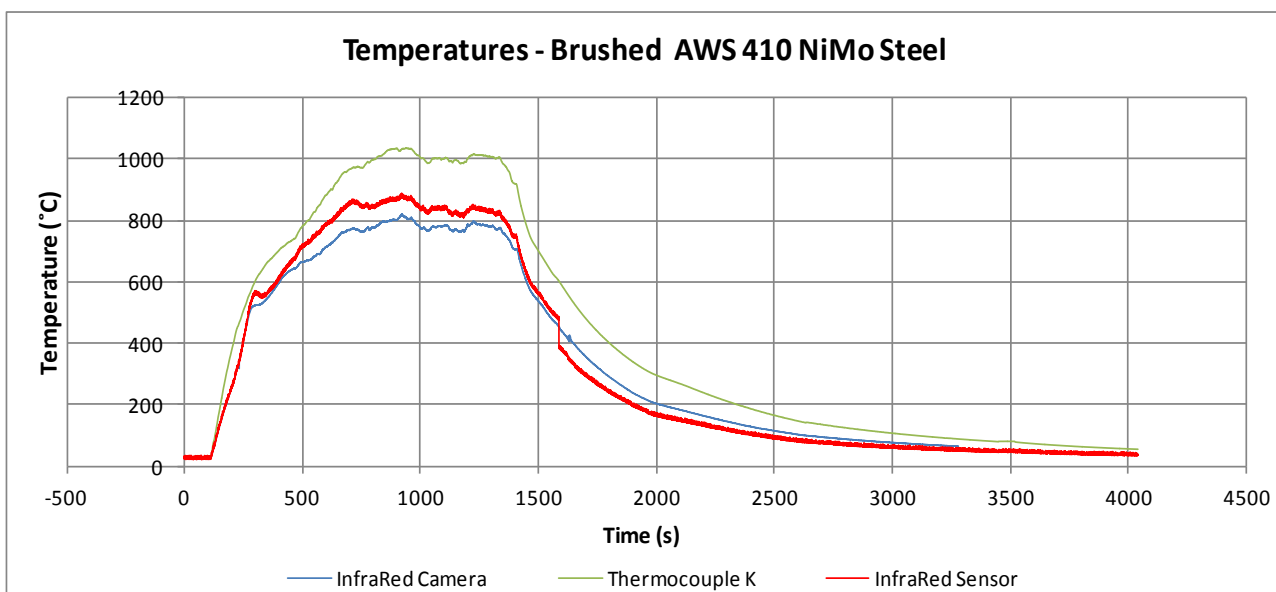


Figure 11: Heating and cooling curves for brushed AWS 410 NiMo.

The cooling curves were close but not as close as those of mild steel. The emissivity is represented in Fig. 12.

Matheus Tabata Santos, Palloma V. Muterlle, Guilherme Caribé de Carvalho, Taygoara F. de Oliveira and Leonardo V. de A. Rusczyk. Experimental Emissivity Determination for the Stainless Steels CA-6NM and 410 NiMo for Application at High Temperatures

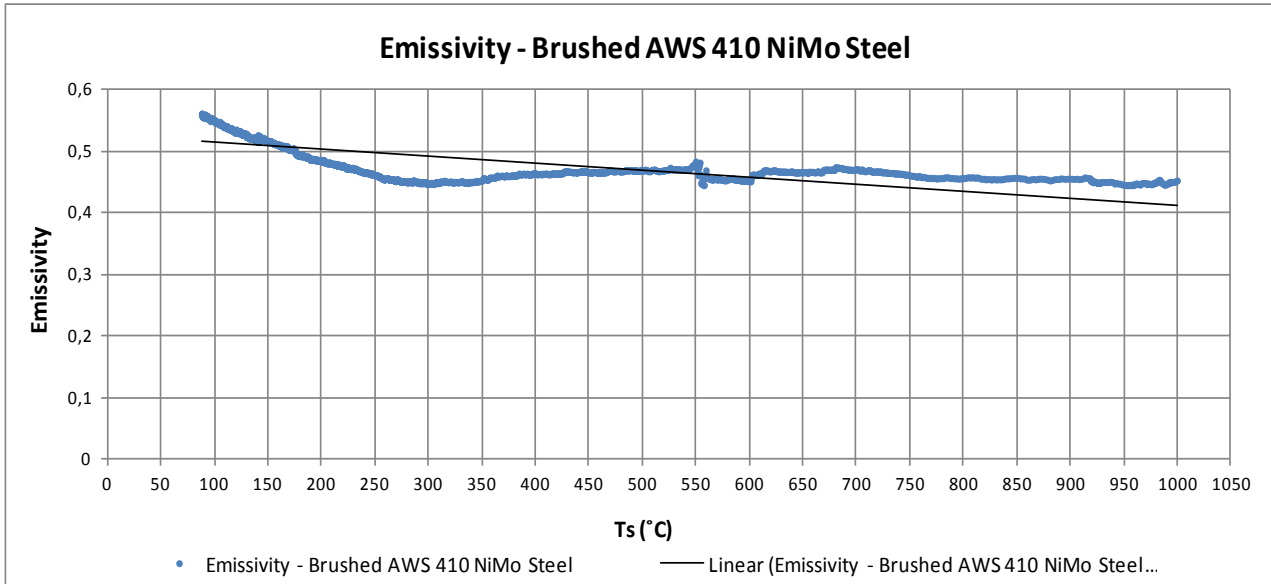


Figure 12: Emissivity curve for brushed AWS 410 NiMo.

After this, the same sample was tested to analyze the response with an oxidized condition. The heating and cooling curves for this is shown in Fig. 13. During heating the temperature values had a significantly discrepancy. This occurred due to the fact that the oxyacetylene flame hit the front face of the sample, disrupting the thermocouple measurements and radiometric sensors.

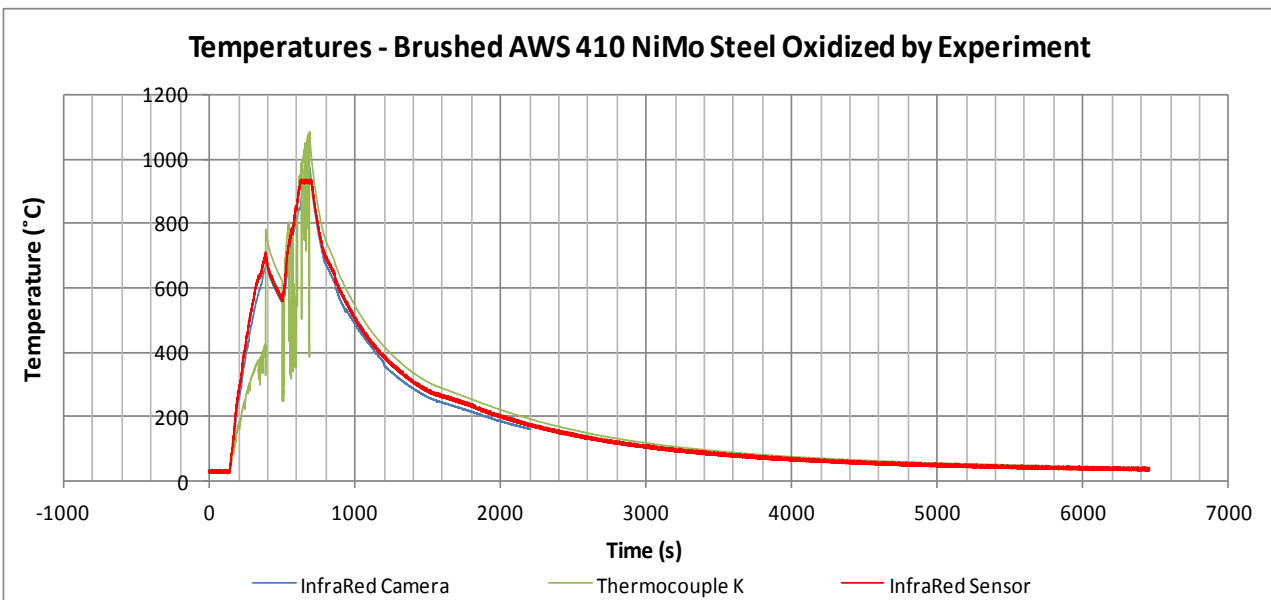


Figure 13: Heating and cooling curves for AWS 410 NiMo steel oxidized by experiment.

The emissivity curve for the Brushed AWS 410 NiMo oxidized by experiment is shown in Fig. 14.

22nd International Congress of Mechanical Engineering (COBEM 2013)
 November 3-7, 2013, Ribeirão Preto, SP, Brazil

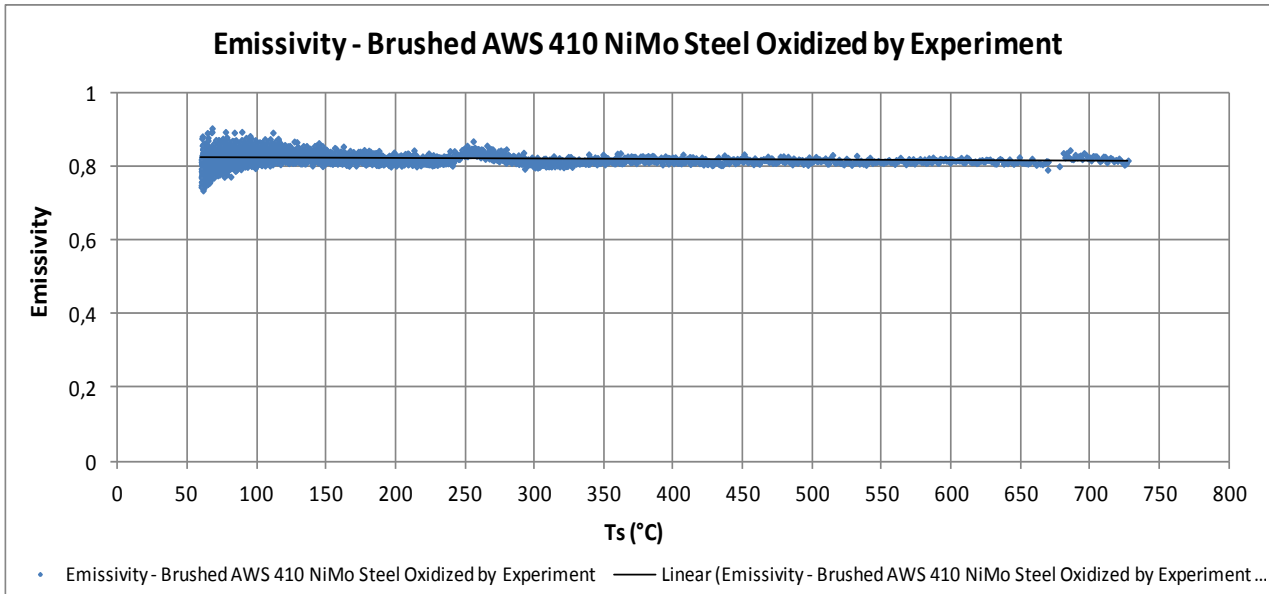


Figure 14: Emissivity curve for AWS 410 NiMo oxidized by experiment.

Figure 14 shows a good linear response to the brushed NiMo 410 stainless steel oxidized sample. The good agreement of the radiometric sensor readings for cooling can be explained by the high emissivity of the oxide layer. The heating and cooling curves for AWS 410 NiMo steel sample (as welded) is illustrated in Fig. 15.

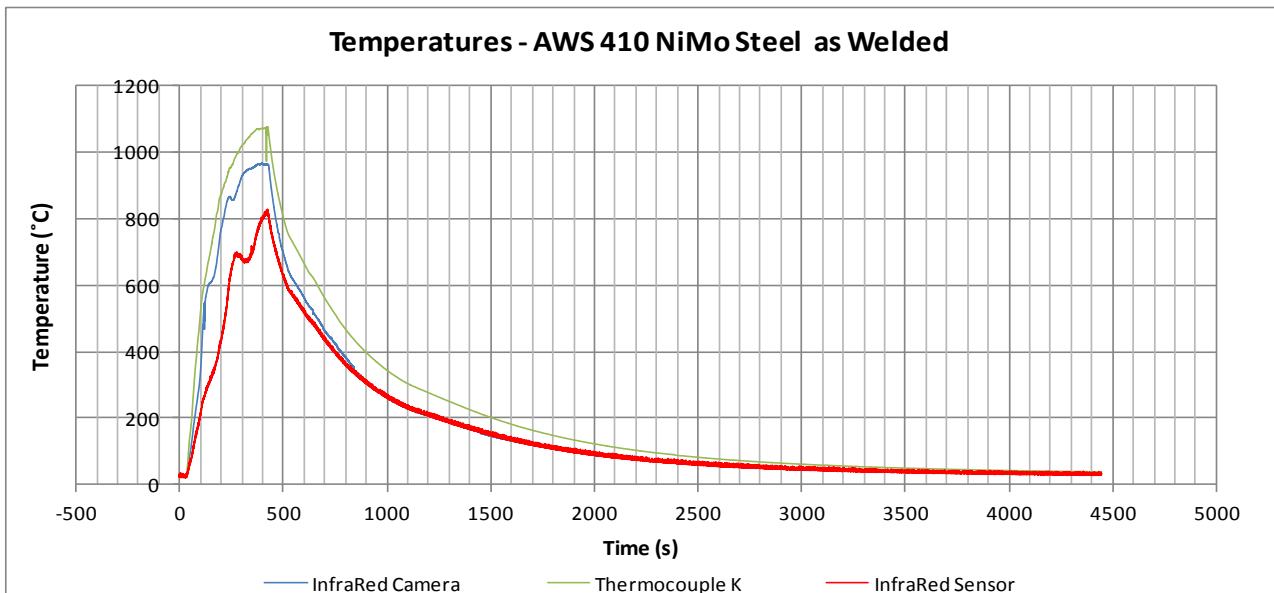


Figure 15: Heating and cooling curves for AWS 410 NiMo as welded.

The emissivity curve for the AWS 410 NiMo (as welded) sample is shown in Fig. 16.

Matheus Tabata Santos, Palloma V. Muterlle, Guilherme Caribé de Carvalho, Taygoara F. de Oliveira and Leonardo V. de A. Ruszczyk. Experimental Emissivity Determination for the Stainless Steels CA-6NM and 410 NiMo for Application at High Temperatures

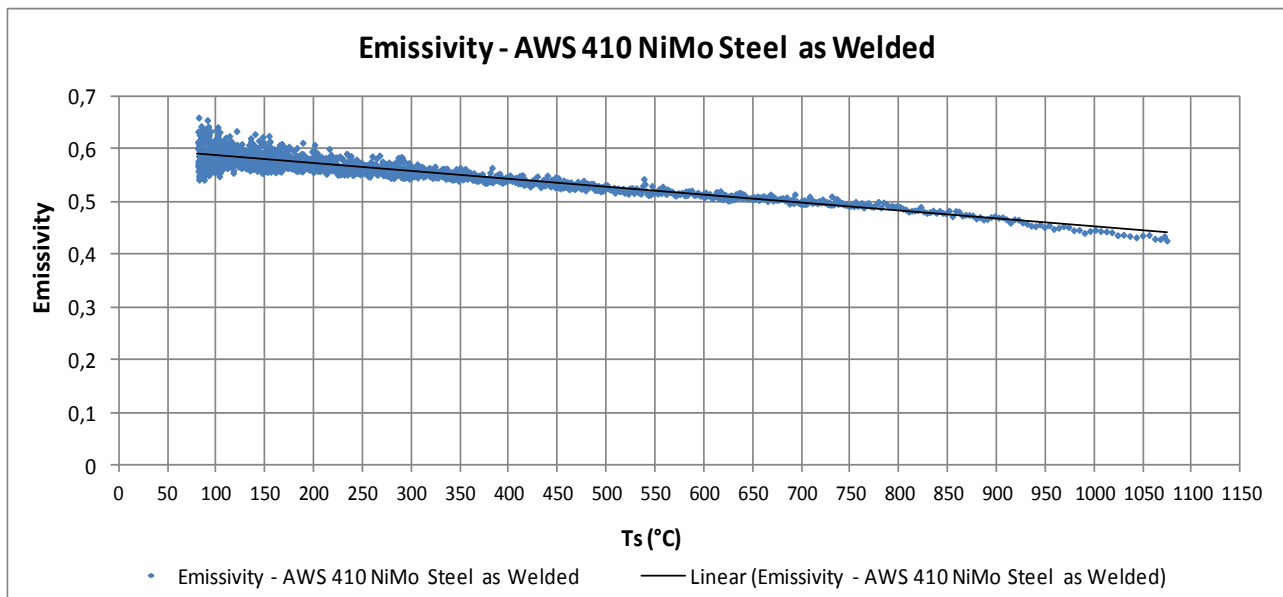


Figure 16: Emissivity curve for AWS 410 NiMo as welded.

5. CONCLUSIONS

Considering the good agreement between the results obtained in this work and the results reported in the literature for similar materials, it can be concluded that the method presented in this paper is a simple and trustworthy technique for determining opaque material emissivities at high temperatures for application in non-contact temperature measurement.

It may be noted that the cooling curves reported by the infrared sensor, with emissivity set as a unit, has a very large proximity to the curves acquired with the temperature data provided by the infrared camera, also with the emissivity parameter set as a unit. This fact shows that the values reported by the infrared sensor are consistent with reality. This can be seen in Figs. 7, 9, 11, 13 and 15.

As shown on Figs. 8, 10, 12, 14 and 16, the emissivity curves showed such little inclination, result of the efficiency of shielding gas.

The fact that the oxyacetylene flame reaches the sample, interfering with the temperature data during heating, was not a problem in determining the emissivity, since only the cooling data were used to calculate the emissivity parameter.

The effect of convection from the shielding gas in thermocouple, which contributes to the temperature readings from the thermocouple are lower than the real temperature of the surface. However, as the gas flow of shielding gas is not high, and we are working at high temperatures, this factor can be considered irrelevant.

The results of this work showed a good response, providing a basis for proper thermographic temperature monitoring.

6. REFERENCES

- BRAMSON, M.A. (1968). *Infrared Radiation, A Handbook for Applications*: Plenum Press, N.Y.
 ÇENGEL, Y. (2003). *Heat Transfer: A practical Approach*. New York: McGrall-Hill, 2nd Edition.
 FLIR Systems. (2004). Thermo Vision A40M Operator's Manual. Suécia.
 INCROPERA et al. (2007). *Fundamentals of Heat and Mass Transfer*. John Wiley & Sons, 6th Edition.

7. RESPONSIBILITY NOTICE

The authors are the only responsible for the printed material included in this paper.